THE JOURNAL OF PHYSICAL CHEMISTRY B

Article

pubs.acs.org/JPCB

Effects of pH and Charge State on Peptide Assembly: The YVIFL Model System

Thanh D. Do,[†] Nichole E. LaPointe,[§] Nicholas J. Economou,[†] Steven K. Buratto,[†] Stuart C. Feinstein,[§] Joan-Emma Shea,[‡,†] and Michael T. Bowers*,[†]

[†]Department of Chemistry and Biochemistry, [‡]Department of Physics and [§]Neuroscience Research Institute and Department of Molecular, Cellular and Developmental Biology, University of California at Santa Barbara, Santa Barbara, California, 93106, United States

Supporting Information

ABSTRACT: Peptide oligomerization is necessary but not sufficient for amyloid fibril formation. Here, we use a combination of experiments and simulations to understand how pH influences the aggregation properties of a small hydrophobic peptide, YVIFL, which is a mutant form of [Leu-5]-Enkephalin. Transmission electron microscopy and atomic force microscopy measurements reveal that this peptide forms small aggregates under acidic conditions (pH = 2), but that extensive fibrillization only occurs under basic conditions (pH = 9 and 11). Ion-mobility mass spectrometry identifies key oligomers in the oligomerization process, which are further characterized at an atomistic level by molecular dynamics simulations. These simulations suggest that terminal charges play a critical role in determining aggregation propensity and aggregate morphology. They also reveal the presence of steric zipper oligomers under basic conditions, a possible precursor to fibril formation. Our experiments suggest that multiple aggregation pathways can lead to YVIFL fibrils, and that cooperative and multibody interactions are key mechanistic elements in the early stages of aggregation.

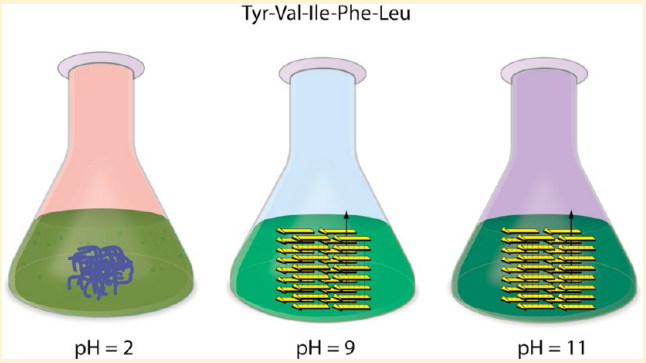

INTRODUCTION

The self-assembly of biomolecules into ordered nanostructures was intensively studied both for biomedical applications (e.g., drug development for the treatment of amyloidoses such as Alzheimer's disease and type II diabetes)[1−4] and bioengineering applications (e.g., tissue engineering[5] and construction of materials with novel biofunctionalities[6,7]). Aggregation is strongly affected by both physicochemical and nonphysicochemical parameters. Physicochemical effects are linked to the crowded cellular environment[8,9] (which contains a host of other molecules including proteins, RNA, polysaccharides, lipids, etc.), the presence of organic osmolytes (e.g., urea[10,11] and trimethylamine N-oxide[12−14] that denature and stabilize globular proteins,[15] respectively), as well as aggregation-promoting macromolecules (e.g., heparin and fatty acids).[16,17] Nonphysicochemical effects include (but are not limited to) pressure, temperature,[18] pH,[19] ionic strength,[20,21] and buffer conditions.[22] These nonphysicochemical parameters, which are often manipulated in *in vitro* experiments to mimic aggregation *in vivo*, can dramatically affect the distribution of oligomer conformations present during assembly. This aspect is difficult to characterize experimentally, as traditional solution techniques measure the average dynamics of the entire system, making differentiation among oligomeric species challenging.

Ion-mobility mass spectrometry (IM-MS) is one of only a few techniques capable of providing structural information about aggregating peptides at a molecular and oligomeric level without external modifications to the system before experiment. This technique permits a determination of the sizes and shapes of individual mass-selected species without convoluting them into a single averaged entity (as would be the case in traditional solution equilibrium studies). It has recently been shown that IM-MS can accurately measure both oligomer distributions and size-dependent oligomer cross sections for various systems including $A\beta_{40}$ and $A\beta_{42}$;[23,24] YGGFL, NNQQNY, SSTNVG and VEALYL;[25] DNA;[26,27] and G-quadruplex.[28−30] More recently, we mutated the sequence of normal [Leu5]-Enkephalin (YGGFL),[31] a nonaggregating pentapeptide known for forming globular oligomers,[25] into YVIFL which can aggregate into fibrillar structures in water at pH = 7. Our analysis demonstrated that the peptide adopts β-sheet structures at the oligomer level (see Supporting Information (SI)). In this present study, IM-MS, transmission electron microscopy (TEM), and atomic force microscopy (AFM) are used to elucidate the effect of acidic and basic pH on

Received: June 19, 2013
Revised: August 9, 2013
Published: August 12, 2013

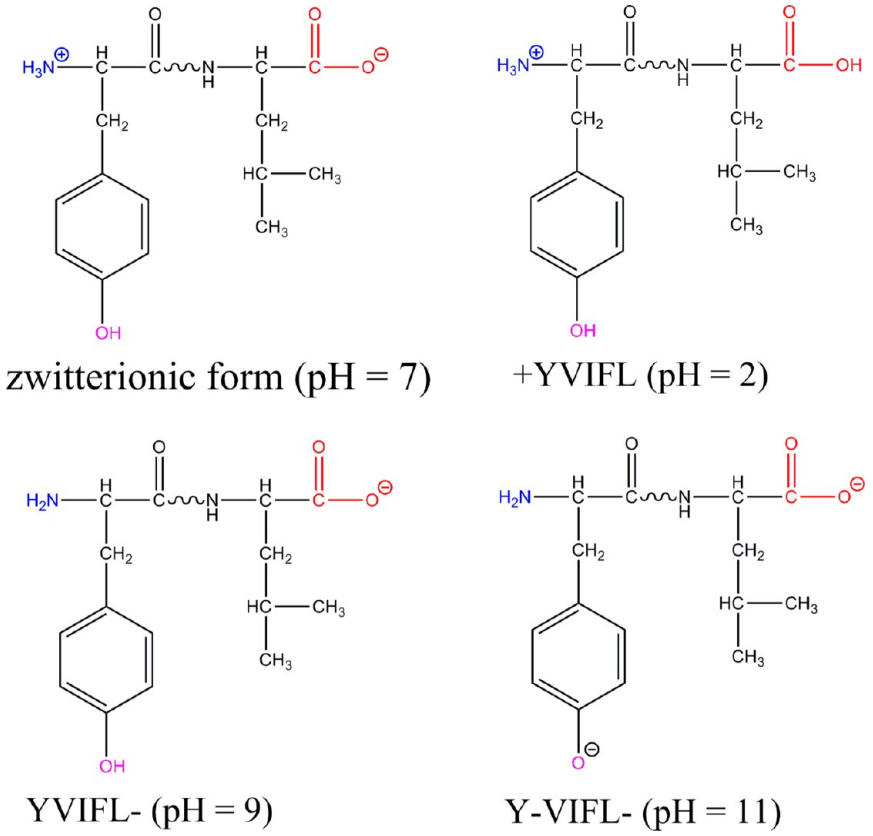

Figure 1. Chemical structures of the YVIFL terminal residues and predicted charge states under different pH conditions.

aggregation rates and morphologies of YVIFL. Molecular dynamics simulations of YVIFL tetramers under pH = 2, 9, and 11 reveal structural differences at the atomic level that give insights into the effects of pH on aggregation propensity.

MATERIALS AND METHODS

Peptides and sample preparation. The free-terminal peptide YVIFL was synthesized by FMOC (*N*-(9-fluorenyl)-methoxycarbonyl) chemistry. The peptide was purified by reverse-phase HPLC and characterized by mass spectrometry and amino acid analysis to confirm the purity and integrity of the peptide. Stock solutions were prepared at 2.0 mg/mL in hexafluoroisopropanol (TCI America, USA) to disrupt oligomer formation and prevent aggregation. Aliquots of stock solution were evaporated overnight before dilution to a final concentration of 200 μM in 20 mM ammonium acetate at pH = 2, 9, or 11. The pH of each buffer was adjusted by ammonium hydroxide or acetic acid. Samples were incubated at room temperature.

The role of charge in YVIFL aggregation can be examined by varying solution pH, as this induces different charge states for the N- and C-termini and the tyrosine side-chain residue.[32] Here we compare three different versions of YVIFL: +YVIFL (very acidic pH = 2, protonated C-terminus), YVIFL− (basic pH = 9, deprotonated N-terminus) and Y−VIFL− (very basic pH = 11, deprotonated N-terminus and tyrosine side chain). The proposed structures and charge states of YVIFL under these pH conditions are shown in Figure 1.

IM-MS. IM-MS is a method capable of detecting multiple conformers and oligomeric species having the same mass to charge (m/z) ratios. Ions are formed from solution by nanoelectrospray ionization (ESI). In traditional MS mode, ions are directly passed through the drift cell to a mass analyzer to obtain a mass spectrum. In IM-MS, ions are captured, stored, and then pulsed into a drift cell filled with a few torr (~13) of helium gas. The ions are drawn through the drift cell by a weak electrical field that is partially balanced by frictional drag created by collisions of analyte ions with buffer gas atoms. As a result, the ions travel with constant velocities as functions of instrumental parameters (e.g., pressure to drift voltage P/V ratios) and their own intrinsic sizes, shapes, and charges. Upon exiting the drift cell the ions are analyzed by MS and an arrival time distribution (ATD) is obtained. The presence of multiple features in the ATD for a specific mass-to-charge ratio (m/z) indicates either multiple conformers at that m/z or multiple oligomers with the same reduced n/z (n = oligomer number, z = charge) or both. The ion velocities can be used to calculate the reduced ion mobility K_0, which is independent of pressure and temperature, and then the experimental collision cross sections σ:[33]

$$K_0 = \frac{(18\pi)^{1/2}}{16}\left[\frac{1}{m} + \frac{1}{m_b}\right]^{1/2} \frac{ze}{(k_B T)^{1/2}} \frac{1}{\Omega_{avg}} \frac{1}{N}$$

where m and m_b are the molecular weights of the ions and buffer gas molecules, respectively, ze is the charge of the ion, N is the buffer gas density, and Ω_{avg} is the rotationally averaged collisional cross section integral, which closely approximates the average collision cross section σ. The IM-MS instrument was built in-house and consists of a nano-ESI source, an ion funnel, a 2-m long drift cell, a second ion funnel, and a quadrupole mass filter.[34]

The relative intensity of an ATD feature reflects the abundance of each species present. For a broad feature

dx.doi.org/10.1021/jp406066d | J. Phys. Chem. B 2013, 117, 10759−10768

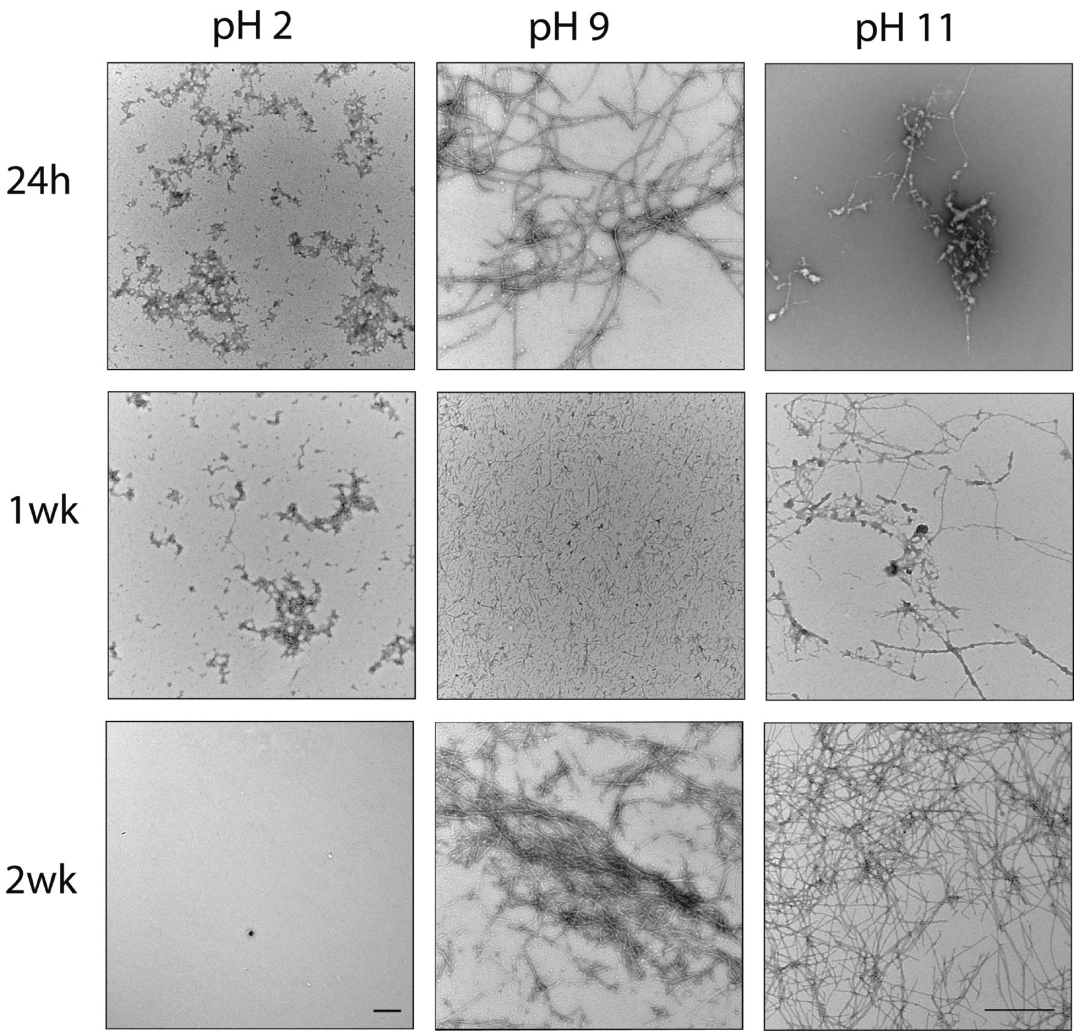

Figure 2. Representative time-course TEM images of 200 μM YVIFL in 20 mM ammonium acetate under different pH conditions. The pH = 2 sample shows the formation of thin flake (amorphous) aggregates which persist in the one-week incubated sample. The pH = 9 sample shows fibril formation after 24 h, shorter but more populated fibrils after one week, and long fibrils after two weeks. The pH = 11 sample forms aggregates with both amorphous and thin needle shapes after 24 h which elongate in the one-week sample. After two weeks, fibrils are abundant. All images are at 50,000× magnification except the two-week pH = 2 image, which is at 10,000× magnification. This lower magnification image covers a larger area of the grid, showing that no aggregates are observed. All scale bars = 500 nm.

containing multiple unresolved conformations, we fit the distribution with a theoretical Gaussian-shape peak using its height and mobility as variables.[27] More details on this process can be found in the SI.

TEM. To begin, 200 μM samples were incubated at room temperature for a minimum of 24 h and up to 2 weeks. To prepare samples for TEM, peptides were fixed in 1.6% glutaraldehyde (Electron Microscopy Sciences) for 15 min at room temperature. A drop of the fixed sample was then placed on a 300-mesh Formvar-coated copper grid (Electron Microscopy Sciences) and allowed to absorb for 1.5 min. After this time, excess sample was wicked away, and the grid was coated with 1 mg/mL cytochrome c for 15 s (to encourage even staining), rinsed with deionized water to remove the cytochrome c, and then negatively stained with 2% uranyl acetate (Ted Pella, Inc.) for 20 s. Grids were viewed on a JEOL-1230 TEM microscope at 80 kV. Digital images were acquired using an ORCA camera and AMT Image Capture Software (version 5.24).

AFM. AFM data were collected for samples at the concentrations of 200 μM and similar incubation time as for TEM. AFM images were collected using an Asylum MFP-3D-SA system (Asylum Research, Santa Barbara, USA). A silicon cantilever (MikroMasch NSC-15) with nominal resonant frequency of 325 kHz and spring constant of 40 N/m was employed in tapping mode. The cantilever was tuned to the resonant frequency at a voltage of 1 V, corresponding to a ~50 nm free amplitude. An amplitude set point ratio (R/R_o) of 75–80% was used to achieve optimal height tracking as well as to keep the tip stably in attractive mode (phase >90°). All images were collected at 1 Hz using 512 × 512 scan points. Images were processed using Igor Pro software and were modified by masking fibrils and then applying a first-order flatten to the height and phase images ("Magic Mask" in MFP3D software). No further image modification was used.

Molecular Dynamics Simulations. Temperature based replica exchange molecular dynamics (T-REMD) simulations of tetramers of YVIFL with the charge states at pH = 2, 9, and 11 shown in Figure 1, were performed using the GROMACS 4.5.5 package[35,36] and the all-atom Optimized Potentials for Liquid Simulations (OPLS-AA) force field[37,38] in TIP3P water.[39] Simulation details can be found in the SI under

dx.doi.org/10.1021/jp406066d | J. Phys. Chem. B 2013, 117, 10759–10768

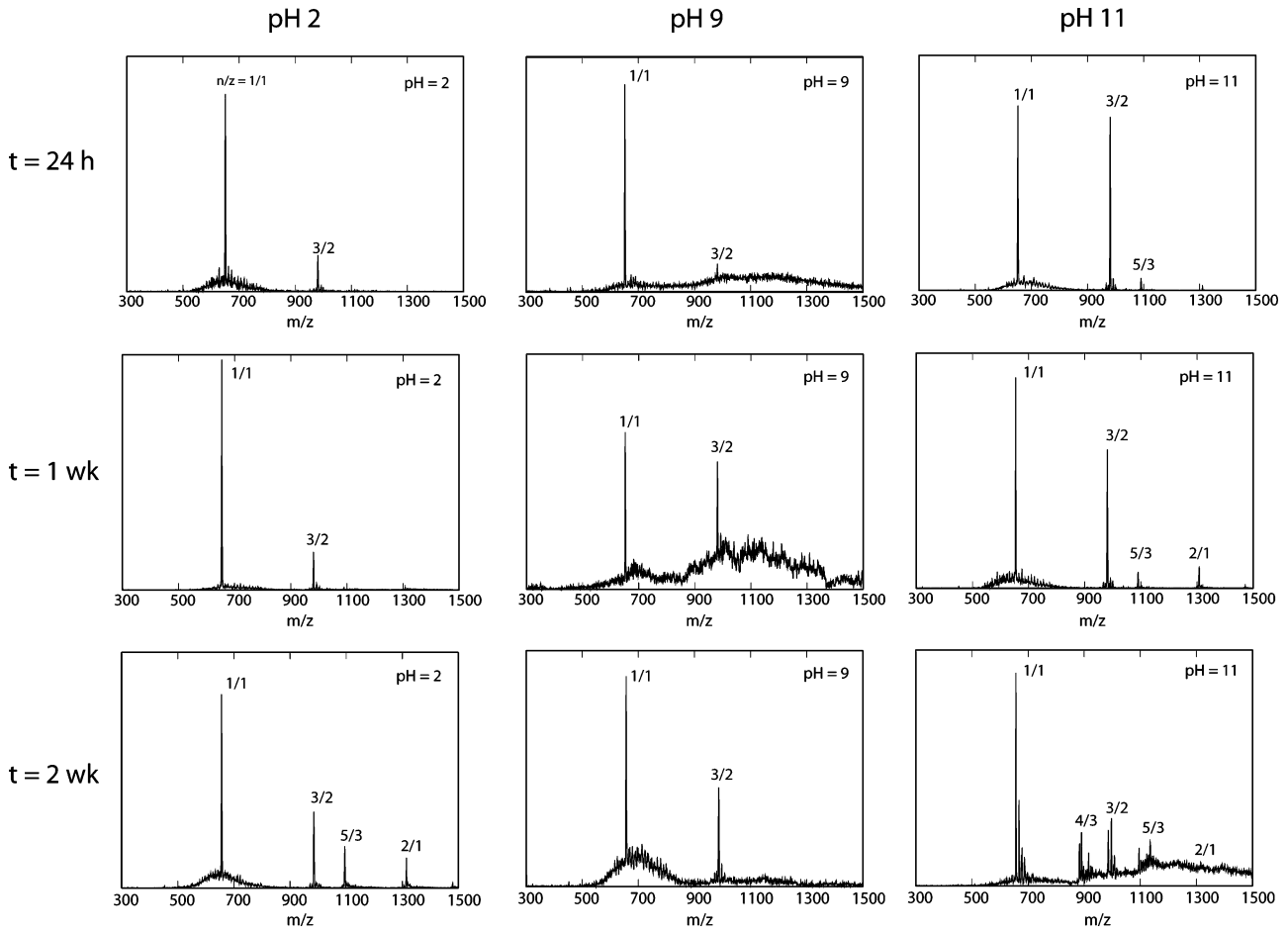

Figure 3. ESI-q-mass spectra obtained during the time-course study (t) of 200 μM YVIFL in 20 mM ammonium acetate under different pH conditions: pH = 2, 9, and 11 (from left to right). In the two aggregation-promoting conditions pH = 9 and pH = 11, low signal-to-noise ratio (S/N) is observed at high m/z, suggesting the presence of unresolved large oligomers. Peak annotations indicate n/z, where n = oligomer size and z = charge.

section S5. A total of 32 replicas were used for each tetramer system. Adjacent replicas attempted exchange after every 2 ps with 20−25% acceptance. The production run was 300 ns per replica. Convergence was assessed by block analysis, and all analyses were performed with the last 100 ns of simulation data.

RESULTS

TEM and AFM Microscopy Data Reveal YVIFL Fibril Formation under Basic Conditions, But Not under Acidic Conditions. TEM images obtained for 24 h, one-week and two-week incubated samples are shown in Figure 2. Aggregates form under all three pH conditions after 24 h, but each pH produces different morphologies. At pH = 2 the aggregates are amorphous and equally distributed across the grid. At pH = 9 long fibrils with an average length of 500 nm are formed. At pH = 11 a mix of nonfibrillar and fibrillar aggregates under 500 nm in length are dispersed unevenly over the grid, with some round aggregates.

After one week of incubation, little change is observed in aggregate morphologies produced at pH = 2 and 11, though there is an overall decrease in the abundance of aggregates at pH = 2 and an increase in the abundance of aggregates at pH = 11. At pH = 9 there is increased formation of short fibrils. The presence of so many shorter fibrils are likely the result of a "clumping" process in which fibrils closely pack to form unequally distributed fibrillar "clusters," as shown in Figure S1 in the SI.

After two weeks of incubation, there continues to be abundant formation of fibrils at pH = 9 while the concentration of aggregates decreases or is eliminated in the pH = 2 solution. Interestingly the pH = 11 solution develops long fibrils at a lower frequency but with similar morphology to those formed at pH = 9. It is important to note that the average dimension (width) of the fibrils obtained under the two basic conditions is approximately 9 nm, close to the 10 nm width that is typical of amyloid fibrils (see Figure S2 in the SI for a dimension comparison of the fibrils).[40]

AFM images (see Figure S3 in the SI) obtained for week-old samples are consistent with TEM data. High resolution AFM suggests the nonfibrillar aggregates formed at pH = 2 are globular. At pH = 9, long and thin fibrils are abundant and equally populated over the surface, confirming that this pH condition strongly promotes fibrillar aggregation. The pH = 11 condition produces a high degree of fibril formation consistent with the TEM observations discussed above.

Ion-Mobility Mass-Spectrometry Shows Distinct Oligomer Sizes for Different pH Conditions. As discussed above, the charges on the YVIFL peptide in solution vary as a function of pH (Figure 1). The positive ion mode ESI-quadrupole-mass spectra of YVIFL solutions at different pH conditions are shown in Figure 3. We note that ESI often

dx.doi.org/10.1021/jp406066d | J. Phys. Chem. B 2013, 117, 10759−10768

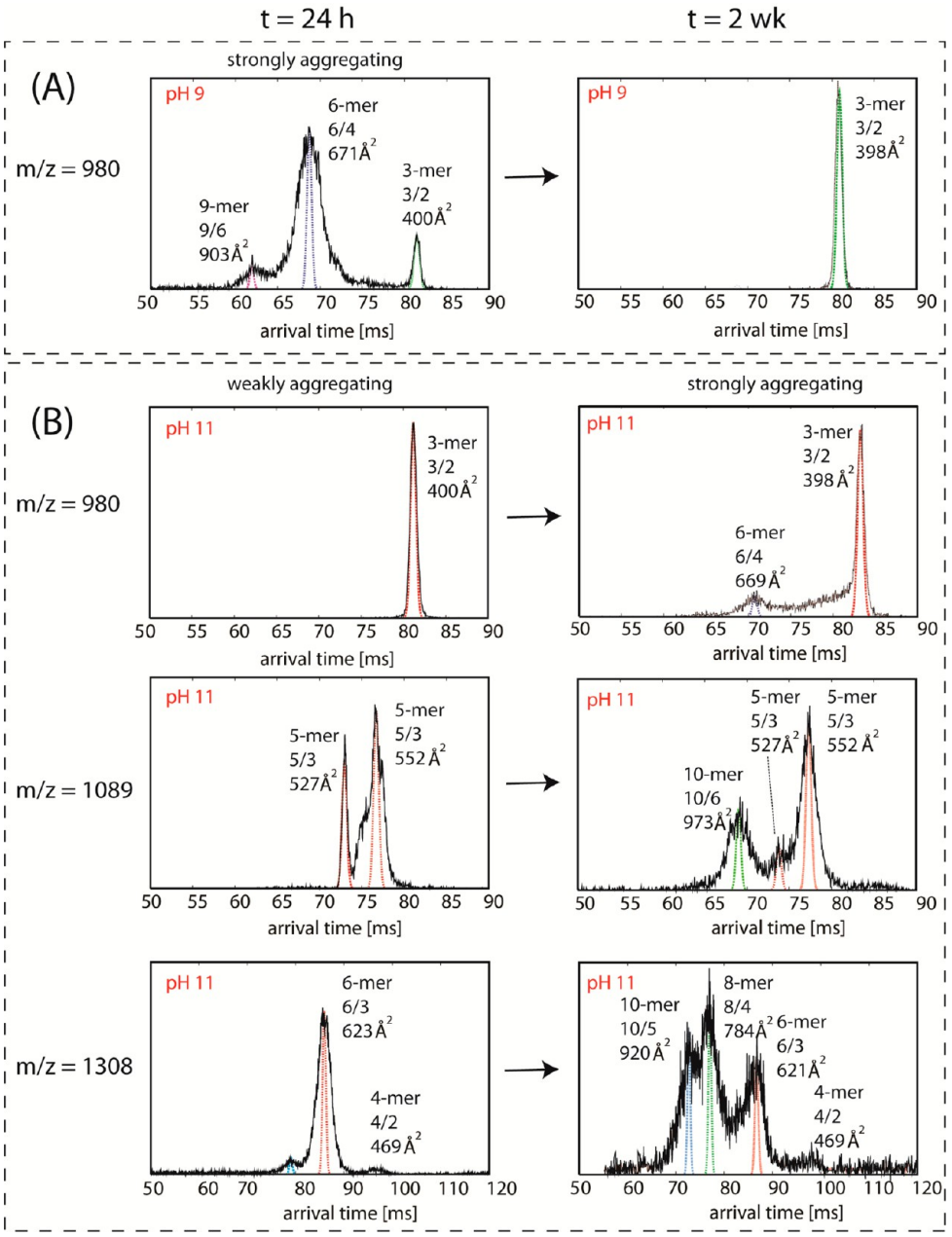

Figure 4. ATDs of the major oligomer peaks obtained from IM-MS experiments for YVIFL under basic conditions. (A) At pH = 9, YVIFL aggregates at time t = 24 h, with the 980 m/z ATD showing the formation of a hexamer and nonamer (left panel). This ATD has simplified after 2 weeks, possibly due to extensive aggregation (right panel). (B) At pH = 11, YVIFL does not aggregate extensively at time t = 24 h (left panel), but after 1 to 2 weeks incubation (right panel), large oligomers are detected by IM-MS, corresponding the extensive fibril formation seen in TEM/AFM.

produces ions whose charges are not directly related to the expected native charges in solution[25,41−45] (see the q-Tof mass spectra in Figure S4 in the SI obtained for the samples in both negative and positive modes). All mass spectra show the formation of early and transient oligomers. Peaks are annotated with their n/z ratios, where n is the oligomer size and z is the charge.

Under acidic conditions, only n/z 1/1 and 3/2 are detected in fresh (t = 24 h) samples (see Figure 3). After two weeks, additional peaks are observed at n/z 5/3 (1090 m/z) and n/z 2/1 (1308 m/z). The ATDs for n/z 5/3 and n/z 2/1 contain features corresponding to the +YVIFL pentamer and hexamer, respectively (see SI section S6).

At pH = 9 distinct peaks are observed at n/z 1/1 (654 m/z) and n/z 3/2 (980 m/z) after 24 h although a broad, unresolved oligomer signal is also present at high m/z. The ATD for n/z 3/2 shows the formation of a hexamer and a nonamer after 24 h (see Figure 4A). However, the signals of these large oligomers are attenuated after additional incubation, suggesting that they quickly oligomerize further to form prefibrillar structures, as evidenced by fibril formation after 24 h (see Figure 2).

Different results are obtained at pH = 11, including a stronger trimer peak (n/z 3/2) and the formation of a pentamer (n/z 5/3) after 24 h (Figure 4B). A tetramer (n/z 4/2) and hexamer (n/z 6/3) were observed after 24 h to one week. Major changes occurred after two weeks, with formation

dx.doi.org/10.1021/jp406066d | J. Phys. Chem. B 2013, 117, 10759−10768

of dodecamer (n/z 10/6 and n/z 10/5) and octamer (n/z 8/4) at empirical n/z values of 5/3 (1090 m/z) and 2/1 (1308 m/z, present but low in intensity). Formation of a dodecamer and octamer is unique to aggregation at pH = 11. Also at two weeks, a small change relative to pH = 9 can be observed at the ATDs of n/z 3/2 (980 m/z), which shows some trace of a hexamer (n/z 6/4). At this longer time point, fibrils with well-defined morphology become visible by TEM/AFM, similar to those observed at pH = 9 (see Figure 2).

The mass spectra at pH = 9 and 11 also show low signal-to-noise (S/N) intensities at high m/z values throughout the two-week study (Figure 3). This suggests the presence of unresolved large oligomers, and correlates to the abundant fibrils observed in TEM and AFM after one and two weeks (see Figure 2 and SI, Figure S3).

Table 1 shows experimental collision cross sections (σ, Å^2) obtained for the oligomers at different pH values. These values

Table 1. Experimental and Isotropic Cross Sections of Oligomers of YVIFL under Different pH Conditions[a]

	experimental cross sections (σ, Å^2)			
oligomer size (n)	pH = 2	pH = 9	pH = 11	isotropic (σ, Å^2)
2	301 (+0.6%)	298 (+0.3%)	297 (+0.0%)	297
3	400 (+2.8%)	400 (+2.8%)	400 (+2.8%)	389
4	n/a	n/a	469 (−0.4%)	471
5	525 (−4.0%), 553 (+1.1%)	n/a	527 (−3.8%), 552 (+1.0%)	546
6	623 (+0.9%)	671 (**+8.7%**)	621 (+0.6%), 669 (**+8.3%**)	617
7	n/a	n/a	n/a	684
8	n/a	n/a	784 (+4.8%)	748
9	n/a	903 (**+12%**)	n/a	809
10	n/a	n/a	920 (**+6.0%**), 973 (**+12%**)	867

[a]The number inside the parentheses is the cross section difference in percentage between the experimental and isotropic cross sections. Cross section deviations greater than 5% are considered significant, indicating possible structural transitions from isotropic oligomers to β-sheet or steric zipper. n/a = not applicable.

are compared to the isotropic cross sections. In the isotropic model, the oligomer grows equally in all spatial dimensions and its cross section is a function of $n^{2/3}$ where n is the oligomer size ($\sigma_{isotropic} = \sigma_1 \times n^{2/3}$, where σ_1 = 187 Å^2 is the experimental cross section of YVIFL monomer). Interestingly, the cross section difference between experiment and the isotropic model becomes significant at large oligomer sizes ($n \geq 6$). The cross section deviations occur for the hexamer and nonamer of YVIFL at pH = 9, and these species, along with hexamer, and decamer under pH = 11 conditions, appear to be the key oligomeric species governing the aggregation. On the other hand, no transition is detected at pH = 2, suggesting that fibrils do not form when the C-terminus is protonated, consistent with the microscopy data.

Molecular Dynamics Simulations. While monomer, dimer, and trimer are observed under both acidic and basic conditions, the YVIFL tetramer is only observed at pH = 11, indicating that this species is less stable at pH = 2 and 9, and may present an important structural feature for the formation of fibrils at very basic pH. Therefore, the tetramer is an interesting context to explore the role of charges on oligomer stability. T-REMD simulations were used to investigate the conformations and other factors influencing the stability of the tetramer. Define secondary structure of proteins (DSSP) analysis[46,47] (Figure S5A in the SI) suggests that the tetramer contains substantial random coil content under all three pH conditions, and that β-sheet structures also contribute significantly (25−45%) to the total population. However, even though similar secondary structure content is observed under all pH conditions, distinct types of β-rich conformations are observed for the YVIFL tetramers at pH = 2, 9, and 11. The unique features of tetramers under each pH condition are described in the following sections.

pH = 2. The +YVIFL tetramer is stabilized through π-stacking interactions of both homo-Phe,Phe and hetero-Phe,Tyr pairwise interactions (see Figure S5B in the SI). These interactions reduce the stability of β-sheet conformations since they compete with the hydrogen-bond network essential for β-sheet formation (see Figure S7 in the SI for +YVIFL tetramer clusters). This type of structures is nonproductive in fibril formation.

pH = 9. The tetramer of YVIFL− at pH = 9 allows a high degree of conformational degeneracy, as shown by similar populations of parallel and antiparallel alignments (see Figure S8 in the SI) with four possible structural configurations for a β-sheet tetramer (↑↑↓↑, ↑↑↓↓, ↓↑↑↓, and ↑↓↑↓) in the five most abundant clusters. Additionally, a significant fraction of the tetramer structures have a steric zipper conformation (~10% of total), as shown in the Potential Mean Force (PMF) plots in Figure 5 and SI, Figure S8. Although ions are included in the simulations, they are not involved in the formation and stabilization of tetramer structures at this pH.

pH = 11. In the case of Y−VIFL− at pH = 11, single β-sheet structures are rarely observed, and steric zippers with buried hydrophobic faces are the favored motifs, accounting for 10% of the total structures (see Figure S9 in the SI). The remaining conformations obtained from T-REMD are mostly unstructured. This result suggests that the peptide has a necessary motif to seed aggregation, but a long lag phase may be required to transform many unstructured oligomers into ordered oligomer seeds. At this pH, ions play a critical role in charge screening and provide an opportunity for negatively charged tyrosine side chains to interact with each other within the steric zipper formation (Figure 6). These tyrosine-ion−tyrosine salt-bridge interactions are vital for the formation of the oligomers including structured (steric zipper) and unstructured conformations. Overall, the presences of steric zippers at pH = 9 and pH = 11 in the simulations are consistent with the high aggregation propensities of YVIFL under these two conditions.

DISCUSSION

Aggregation Mechanisms Involve Multibody Interactions within Multiple Pathways. Our experimental data reveal a variety of aggregation rates and morphologies for YVIFL in response to different pH conditions. Observations from IM-MS experiments are consistent with TEM and AFM data, and provide new insights into the pH-dependent aggregation of YVIFL. Under basic conditions (pH 9 and 11), we observe the formation of large oligomers ($n \geq 6$) with cross sections that deviate significantly from the isotropic model (see Table 1). This suggests that nucleation of fibril formation occurs in the early assembly stages. In addition, only some specific oligomers are detected prior to and during fibril formation. For example, at pH = 9, *only* dimer, trimer, hexamer, and nonamer are observed in the same time window when

dx.doi.org/10.1021/jp406066d | J. Phys. Chem. B 2013, 117, 10759−10768

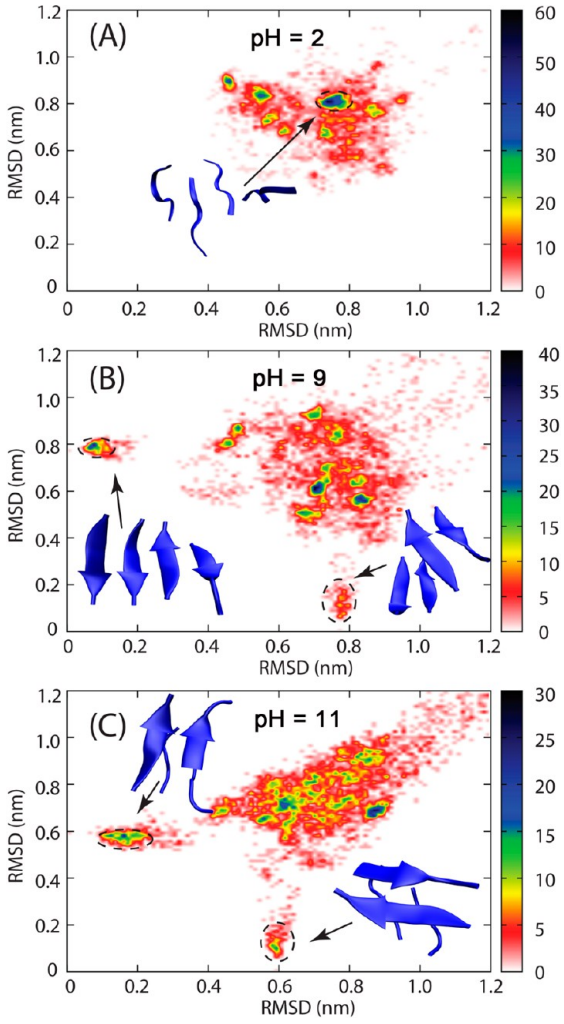

Figure 5. Potential mean force plots display the probabilities and representative conformations for tetramers of (A) +YVIFL (pH = 2), (B) YVIFL− (pH = 9), and (C) Y−VIFL− (pH = 11). The probability distribution was computed according to the backbone RMSD of each conformation from the reference structures. For pH = 2 and pH = 9, the two reference structures are an extended β-sheet (x-axis) and a steric zipper (y-axis). For pH = 11, the two reference structures are two different steric zipper conformations. The cutoff for clustering was 0.3 nm. The most dominant population of +YVIFL (pH = 2) is shown. The populations of β-sheet and steric zippers of YVIFL− (pH = 9) and Y−VIFL− (pH = 11) are also reported.

fibrils are found. At pH = 11, tetramer and hexamer are detected after one week, but regular fibrils are not yet abundant at that point. IM-MS after two-week incubation shows the appearance of octamer (n/z 8/4), decamer (n/z 10/5 and 10/6), and a second hexamer (n/z 6/4), and microscopy reveals the extensive formation of fibrils (Figures 2 and 4). These observations indicate that the formation of aggregation-prone oligomers (oligomers with β-sheet character) is highly dependent upon the formation of specific precursors, rather than being a consequence of a single monomer addition to an existing oligomer. The morphology of aggregates formed at pH = 11 suggests the aggregation mechanism shares common features both with the pH = 2 results (i.e., the initial formation of amorphous aggregates) and with the pH = 9 results (i.e., fibril formation after long incubation) (see Figure 2). Long incubation times favor fibril formation, suggesting possible

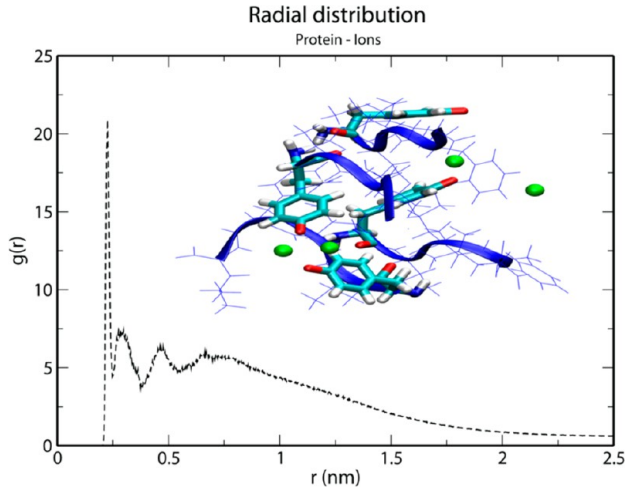

Figure 6. Ions play an important role in stabilizing the steric zipper structures at pH = 11 through attraction to the negatively charged tyrosine residues. The radial distribution $g(r)$ of the protein−ion has a most probable distance of 2.5 Å indicating significant interactions. A representative steric zipper conformation with two sodium cations (green) coordinating each negatively charged tyrosine side chain is shown.

multiple pathways and similar but not identical fibril structures under these different pH conditions.

Conformational Degeneracies and Steric Zipper Formation Play Essential Roles in Assisting Fibril Formation. Previous studies of pH-dependent aggregation[48−50] suggest that subtle factors determine a peptide's aggregation propensity. Characteristics such as salt bridges, hydrogen-bond networks, hydrophobicity, and net charge contributions from ionizable side chains have been considered the prevailing driving forces in the classical picture of aggregation. A correlation between low net charge and high aggregation propensity is assumed to underlie the conventional attraction−repulsion model, in which charged residues not only interrupt contiguous stretches of hydrophobic sequences but also create electrostatic repulsions between monomer units.[51] However, the importance of terminal net charge in regulating aggregation propensity is often overlooked as compared to ionizable residue side chains.[52] The difference between our peptide model and those studied in previous works lies in the simplicity of the charge state modification. In our model, a very hydrophobic peptide yields distinct aggregation outcomes depending on pH: globular/amorphous aggregates under pH = 2 and fibrillar aggregates under pH = 9 and 11. In addition to charge state, additional components that regulate aggregation behavior include conformational degeneracies[48] (i.e., the possibility of oligomers adopting mixed parallel/antiparallel configurations), solvent effects, and the accessibility of oligomers to certain aggregation-prone conformations.[53] The complex interplay of molecular interactions promoting or suppressing the aggregation propensity of YVIFL is limited to (1) ionic strength and electrostatic interactions, (2) conformational fluctuations and degeneracies due to terminal and tyrosine charges, and (3) the ability to form β-sheet structures (e.g., single β-sheet or steric zipper).

A relatively low pH condition can weaken both electrostatic and hydrogen bonding components of the terminal salt-bridges (i.e., interacting NH_3^+...COO^- pairs are replaced by NH_3^+...COOH), thus potentially reducing aggregation. Exper-

dx.doi.org/10.1021/jp406066d | J. Phys. Chem. B 2013, 117, 10759−10768

imental results suggest that only amorphous aggregates are seen at pH = 2, which is consistent with no structural transitions at this pH. In addition, microscopy data suggests the peptide may undergo polymerization into unstructured aggregates and/or an irreversible denaturation into inactive, nonaggregating species,[54] evidenced by the decrease in abundance of large aggregates after one week.

Under the aggregation-promoting condition (pH = 9), the tetramer adopts both parallel and antiparallel β-structures. In contrast, the zwitterionic tetramer structure (+YVIFL−) at neutral pH preferentially adopts only the antiparallel type of β-structures (see Figures S14 and S15 in the SI). Therefore, the higher aggregation propensity of YVIFL− (pH = 9) relative to the zero net charge state (pH = 7) is partially attributed to conformational degeneracies. Specifically, the fact that the peptide chains can access both antiparallel and parallel configurations at pH = 9 leads to an entropic stabilization for assembly.[48] In contrast to this entropic component, the energetic component favors the zero valency peptide, since ionic groups can interact favorably within the solvent. However, with the increase in probability for the oligomers to gain access to both parallel and antiparallel alignments, the pH = 9 system can compensate for energetic loss by entropic gain. Entropic stabilization may also allow the pH = 9 system to potentially avoid kinetic trapping as oligomers grow, thus reaching nucleation faster. In theory, both +YVIFL (pH = 2) and YVIFL− (pH = 9) have similar access to parallel and antiparallel configurations. However, the +YVIFL tetramer structures (see Figure S7 in the SI) do not support the intensive hydrogen-bond networking required for stabilizing a β-sheet, resulting in a weak aggregation propensity.

The formation of steric zipper structures is only observed under basic conditions (pH = 9 and 11). This fact, in combination with the experimental observation that the peptide aggregates much faster under basic conditions than under neutral or acidic conditions, supports the idea that steric zipper formation is important in YVIFL aggregation. While the steric zipper at pH = 9 is stabilized through hydrophobic interactions between β-sheet dimers, steric zipper stability at pH = 11 depends on the presence of positively charged ions. Without the ions, the like-charge repulsion between negatively charged tyrosine side chains may reduce aggregation propensity. However, the presence of positively charged ammonium ions (in experiment) or sodium cations (in simulation) can coordinate those negative charges, and the solvent electrostatic response can attenuate like-charge repulsion and promote slight attraction.[50] Thus, ions can help align the peptide chains by acting as "binding clips" between negatively charged tyrosine pairs, thereby promoting aggregation through steric zipper formation. This is evidenced by the cross section deviation from the isotropic model in IM-MS experiments and by the simulations at pH = 11. Although the early oligomer species at pH = 11 may lack β-sheet character, they are able to adopt prefibrillar structures as they grow larger in size. This is shown by the conversion from globular to fibrillar aggregates observed at the mesoscopic level by microscopy. It is also noted that the pK_a of the tyrosine side chain ($pK_a = 10.3 \pm 1.2$)[32] can depend on the surrounding environment, hence we cannot eliminate the possibility that both YVIFL− and Y−VIFL− coexist under this condition. In either case, fibril formation is an expected consequence.

Oligomerization Does Not *Always* Lead to Larger Aggregates or Fibril Formation. On the basis of the presented data, we propose that aggregation propensity depends on a combination of two important factors: (1) oligomerization rate and (2) the existence of a structural transition. These two coherently integrated factors are the foci of the aggregation cascade. Peptides which do not assemble into structured aggregates would likely have no structural transitions at the oligomer level (e.g., YGGFL).[25] We note that peptides can oligomerize, but not necessarily aggregate further into amorphous or fibrillar aggregates. Indeed, soluble oligomers are observed even if the system has no tendency to form large aggregates.[25,55,56] Thus, oligomerization *per se* does not imply high aggregation propensity. Here we define oligomerization as the process occurring *before* full-fledged aggregation; in other words, before some nucleation event(s) that lead to aggregation. For systems that aggregate, the relationship between oligomerization and aggregation propensity has been considered in a number of theoretical models, some of which have firm grounding in experiment (for instance, template-assisted assembly,[57] nucleated polymerization,[58] and nucleated conformational conversion).[59] These models agree on a crucial point, that the aggregation process is driven by one (or more) rate-determining step(s) that control how quickly fibrils appear. The transition from peptide oligomerization to aggregation can proceed through a variety of pathways, only a few of which can lead to fibril formation. On the other hand, fibril formation can proceed from very different initial states (e.g., YVIFL at pH = 9 and 11).[60]

CONCLUSIONS

Our data suggest the following:

(1) Fibril-formation propensity depends upon the ability of the peptide and its oligomers to adopt certain aggregation-prone conformations (i.e., β-sheet and steric zipper).

(2) Terminal net charges can strongly influence the aggregation propensity of hydrophobic peptides. Adjusting the pH changes the overall charge state on YVIFL from +1 (pH = 2) to −1 (pH = 9) and to −2 (pH = 11). Both ion mobility and TEM indicate very different aggregation rates and outcomes for these three charge states: slow and amorphous aggregation for acidic conditions and faster and β-sheet transitions for basic conditions.

(3) Conformational degeneracy can be important. At pH = 9, while electrostatics support antiparallel stacking, ionic/solvent screening and conformational degeneracy (entropy) support mixed stacking (observed in MD simulations), promoting eventual fibril formation.

ASSOCIATED CONTENT

Supporting Information

Additional details about IM-MS experimental procedure, ATD assignments, T-REMD protocol, and simulation parameters, fibril width analysis, AFM images, Q-tof mass spectra; TEM and T-REMD tetramer structures of YVIFL tetramer at neutral pH = 7. This material is available free of charge via the Internet at http://pubs.acs.org.

AUTHOR INFORMATION

Corresponding Author

*E-mail: bowers@chem.ucsb.edu. Tel: +1-805-893-2673.

Notes

The authors declare no competing financial interest.

■ ACKNOWLEDGMENTS

This research was funded by the National Science Foundation under Grant CHE-0909743 to M.T.B. and by the David and Lucile Packard Foundation and the NSF (MCB 0642086 and 1158577) to J.-E.S. The authors thank Ms. Margaret Condron and Dr. David B. Teplow at UCLA for supplying the peptide. We acknowledge support from the Center for Scientific Computing at the CNSI and MRL under NSF Grants DMR-1121053 and CNS-0960316. This research was also supported in part by the National Science Foundation through TeraGrid resources provided by the Texas Advanced Computing Center under Grant No. TG-CHE130004 to M.T.B. and Grant No. TG-MCA05S027 to J.-E.S. N.J.E. acknowledges a National Science Foundation Graduate Student Research Fellowship. S.K.B. acknowledges funding from the MURI and DURIP programs of the U.S. Army Research Laboratory and U.S. Army Research Office under Grant Nos. DAAD 19-03-1-0121 and W911NF-09-1-0280 for purchase of the AFM instrument. We also acknowledge the use of the NRI-MCDB Microscopy Facility at UC, Santa Barbara.

■ REFERENCES

(1) Eisenberg, D.; Nelson, R.; Sawaya, M. R.; Balbirnie, M.; Sambashivan, S.; Ivanova, M. I.; Madsen, A. O.; Riekel, C. The Structural Biology of Protein Aggregation Diseases: Fundamental Questions and Some Answers. *Acc. Chem. Res.* **2006**, *39*, 568−575.

(2) Cleary, J. P.; Walsh, D. M.; Hofmeister, J. J.; Shankar, G. M.; Kuskowski, M. A.; Selkoe, D. J.; Ashe, K. H. Natural Oligomers of the Amyloid-β Protein Specifically Disrupt Cognitive Function. *Nat. Neurosci.* **2004**, *8*, 79−84.

(3) Murphy, R. M. Peptide Aggregation in Neurodegenerative Diseases. *Ann. Rev. Biomed. Eng.* **2002**, *4*, 155−174.

(4) Adler-Abramovich, L.; Vaks, L.; Carny, O.; Trudler, D.; Magno, A.; Caflisch, A.; Frenkel, D.; Gazit, E. Phenylalanine Assembly into Toxic Fibrils Suggests Amyloid Etiology in Phenylketonuria. *Nat. Chem. Biol.* **2012**, *8*, 701−706.

(5) Hartgerink, J. D.; Beniash, E.; Stupp, S. I. Self-Assembly and Mineralization of Peptide-Amphiphile Nanofibers. *Science* **2001**, *294*, 1684−1688.

(6) Zhang, S. G. Fabrication of Novel Biomaterials through Molecular Self-Assembly. *Nat. Biotechnol.* **2003**, *21*, 1171−1178.

(7) Liu, L. H.; Xu, K. J.; Wang, H. Y.; Tan, P. K. J.; Fan, W. M.; Venkatraman, S. S.; Li, L. J.; Yang, Y. Y. Self-Assembled Cationic Peptide Nanoparticles as an Efficient Antimicrobial Agent. *Nat. Nanotechnol.* **2009**, *4*, 457−463.

(8) White, D. A.; Buell, A. K.; Knowles, T. P.; Welland, M. E.; Dobson, C. M. Protein Aggregation in Crowded Environments. *J. Am. Chem. Soc.* **2010**, *132*, 5170−5175.

(9) Magno, A.; Caflisch, A.; Pellarin, R. Crowding Effects on Amyloid Aggregation Kinetics. *J. Phys. Chem. Lett.* **2010**, *1*, 3027−3032.

(10) Mukrasch, M. D.; Bibow, S.; Korukottu, J.; Jeganathan, S.; Biernat, J.; Griesinger, C.; Mandelkow, E.; Zweckstetter, M. Structural Polymorphism of 441-Residue Tau at Single Residue Resolution. *PLoS Biol.* **2009**, *7*, 399−414.

(11) Deyoung, L. R.; Dill, K. A.; Fink, A. L. Aggregation and Denaturation of Apomyoglobin in Aqueous Urea Solutions. *Biochemistry* **1993**, *32*, 3877−3886.

(12) Cho, S. S.; Reddy, G.; Straub, J. E.; Thirumalai, D. Entropic Stabilization of Proteins by TMAO. *J. Phys. Chem. B* **2011**, *115*, 13401−13407.

(13) Celinski, S. A.; Scholtz, J. M. Osmolyte Effects on Helix Formation in Peptides and the Stability of Coiled-Coils. *Protein Sci.* **2002**, *11*, 2048−2051.

(14) Scaramozzino, F.; Peterson, D. W.; Farmer, P.; Gerig, J. T.; Graves, D. J.; Lew, J. TMAO Promotes Fibrillization and Microtubule Assembly Activity in the C-Terminal Repeat Region of Tau. *Biochemistry* **2006**, *45*, 3684−3691.

(15) Bennion, B. J.; Daggett, V. Counteraction of Urea-Induced Protein Denaturation by Trimethylamine N-Oxide: A Chemical Chaperone at Atomic Resolution. *Proc. Natl. Acad. Sci. U.S.A.* **2004**, *101*, 6433−6438.

(16) Paudel, H. K.; Li, W. Heparin-Induced Conformational Change in Microtubule-Associated Protein Tau as Detected by Chemical Cross-Linking and Phosphopeptide Mapping. *J. Biol. Chem.* **1999**, *274*, 8029−8038.

(17) King, M. E.; Ahuja, V.; Binder, L. I.; Kuret, J. Ligand Dependent Tau Filament Formation: Implications for Alzheimer's Disease Progression. *Biochemistry* **1999**, *38*, 14851−14859.

(18) Goossens, K.; Haelewyn, J.; Meersman, F.; De Ley, M.; Heremans, K. Pressure- and Temperature-Induced Unfolding and Aggregation of Recombinant Human Interferon-Gamma: A Fourier Transform Infrared Spectroscopy Study. *Biochem. J.* **2003**, *370*, 529−535.

(19) Peralvarez-Marin, A.; Barth, A.; Graslund, A. Time-Resolved Infrared Spectroscopy of pH-Induced Aggregation of the Alzheimer Aβ(1−28) Peptide. *J. Mol. Biol.* **2008**, *379*, 589−596.

(20) Arnaudov, L. N.; de Vries, R. Strong Impact of Ionic Strength on the Kinetics of Fibrilar Aggregation of Bovine Beta-Lactoglobulin. *Biomacromolecules* **2006**, *7*, 3490−3498.

(21) Yoshimura, Y.; Lin, Y. X.; Yagi, H.; Lee, Y. H.; Kitayama, H.; Sakurai, K.; So, M.; Ogi, H.; Naiki, H.; Goto, Y. Distinguishing Crystal-Like Amyloid Fibrils and Glass-Like Amorphous Aggregates from Their Kinetics of Formation. *Proc. Natl. Acad. Sci. U.S.A.* **2012**, *109*, 14446−14451.

(22) Kameoka, D.; Masuzaki, E.; Ueda, T.; Imoto, T. Effect of Buffer Species on the Unfolding and the Aggregation of Humanized IGg. *J. Biochem.* **2007**, *142*, 383−391.

(23) Bernstein, S. L.; Dupuis, N. F.; Lazo, N. D.; Wyttenbach, T.; Condron, M. M.; Bitan, G.; Teplow, D. B.; Shea, J.-E.; Ruotolo, B. T.; Robinson, C. V.; Bowers, M. T. Amyloid-β Protein Oligomerization and the Importance of Tetramers and Dodecamers in the Aetiology of Alzheimer's Disease. *Nat. Chem.* **2009**, *1*, 326−331.

(24) Bernstein, S. L.; Wyttenbach, T.; Baumketner, A.; Shea, J.-E.; Bitan, G.; Teplow, D. B.; Bowers, M. T. Amyloid β-Protein: Monomer Structure and Early Aggregation States of Aβ42 and Its Pro^{19} Alloform. *J. Am. Chem. Soc.* **2005**, *127*, 2075−2084.

(25) Bleiholder, C.; Dupuis, N. F.; Wyttenbach, T.; Bowers, M. T. Ion Mobility-Mass Spectrometry Reveals a Conformational Conversion from Random Assembly to Beta-Sheet in Amyloid Fibril Formation. *Nat. Chem.* **2011**, *3*, 172−177.

(26) Gidden, J.; Baker, E. S.; Ferzoco, A.; Bowers, M. T. Structural Motifs of DNA Complexes in the Gas Phase. *Int. J. Mass Spectrom. Ion Proc.* **2005**, *240*, 183−193.

(27) Gidden, J.; Ferzoco, A.; Baker, E. S.; Bowers, M. T. Duplex Formation and the Onset of Helicity in Poly d(CG)$_n$ Oligonucleotides in a Solvent-Free Environment. *J. Am. Chem. Soc.* **2004**, *126*, 15132−15140.

(28) Baker, E. S.; Bernstein, S. L.; Gabelica, V.; De Pauw, E.; Bowers, M. T. G-Quadruplexes in Telomeric Repeats Are Conserved in a Solvent-Free Environment. *Int. J. Mass. Spectrom.* **2006**, *253*, 225−237.

(29) Baker, E. S.; Bernstein, S. L.; Bowers, M. T. Structural Characterization of G-Quadruplexes in Deoxyguanosine Clusters Using Ion Mobility Mass Spectrometry. *J. Am. Soc. Mass Spectrom.* **2005**, *16*, 989−997.

(30) Gabelica, V.; Baker, E. S.; Teulade-Fichou, M. P.; De Pauw, E.; Bowers, M. T. Stabilization and Structure of Telomeric and C-Myc Region Intramolecular G-Quadruplexes: The Role of Central Cations and Small Planar Ligands. *J. Am. Chem. Soc.* **2007**, *129*, 895−904.

(31) Smith, G. D.; Griffin, J. F. Conformation of [Leu5] Enkephalin from X-Ray Diffraction: Features Important for Recognition at Opiate Receptor. *Science* **1978**, *199*, 1214−1216.

(32) Grimsley, G. R.; Scholtz, J. M.; Pace, C. N. A Summary of the Measured pK Values of the Ionizable Groups in Folded Proteins. *Protein Sci.* **2009**, *18*, 247−251.
(33) Mason, E. A. *Transport Properties of Ions in Gases*, 99 ed.; John Wiley & Sons: New York, 1988.
(34) Kemper, P. R.; Dupuis, N. F.; Bowers, M. T. A New, Higher Resolution, Ion Mobility Mass Spectrometer. *Int. J. Mass. Spectrom.* **2009**, *287*, 46−57.
(35) Hess, B.; Kutzner, C.; Spoel, D. v. d.; Lindahl, E. Gromacs 4: Algorithms for Highly Efficient, Load-Balanced, and Scalable Molecular Simulation. *J. Chem. Theory Comput.* **2008**, *4*, 435−437.
(36) Spoel, D. V. D.; Lindahl, E.; Hess, B.; Groenhof, G.; Mark, A. E.; Berendsen, H. J. C. Gromacs: Fast, Flexible, and Free. *J. Comput. Chem.* **2005**, *26*, 1701−1718.
(37) Jorgensen, W. L.; Tiradorives, J. The OPLS Potential Functions for Proteins—Energy Minimizations for Crystals of Cyclic-Peptides and Crambin. *J. Am. Chem. Soc.* **1988**, *110*, 1657−1666.
(38) Kaminski, G. A.; Friesner, R. A.; Tirado-Rives, J.; Jorgensen, W. L. OPLS-AA/L Force Field for Proteins: Using Accurate Quantum Mechanical Data. *Abstr. Pap. Am. Chem. Soc.* **2000**, *220*, U279−U279.
(39) Jorgensen, W. L.; Chandrasekhar, J.; Madura, J. D.; Impey, R. W.; Klein, M. L. Comparison of Simple Potential Functions for Simulating Liquid Water. *J. Chem. Phys.* **1983**, *79*, 926−935.
(40) Sipe, J. D.; Cohen, A. S. Review: History of the Amyloid Fibril. *J. Struct. Biol.* **2000**, *130*, 88−98.
(41) Iavarone, A. T.; Williams, E. R. Mechanism of Charging and Supercharging Molecules in Electrospray Ionization. *J. Am. Chem. Soc.* **2003**, *125*, 2319−2327.
(42) Leblanc, J. C. Y.; Wang, J. Y.; Guevremont, R.; Siu, K. W. M. Electrospray Mass-Spectra of Protein Cations Formed in Basic Solutions. *Org. Mass. Spectrom.* **1994**, *29*, 587−593.
(43) Kelly, M. A.; Vestling, M. M.; Fenselau, C. C.; Smith, P. B. Electrospray Analysis of Proteins—A Comparison of Positive-Ion and Negative-Ion Mass-Spectra at High and Low pH. *Org. Mass. Spectrom.* **1992**, *27*, 1143−1147.
(44) Larini, L.; Gessel, M. M.; Lapointe, N. E.; Do, T. D.; Bowers, M. T.; Feinstein, S. C.; Shea, J. E. Initiation of Assembly of Tau(273−284) and Its ΔK280 Mutant: An Experimental and Computational Study. *Phys. Chem. Chem. Phys.* **2013**, *15*, 8916−8928.
(45) Do, T. D.; Economou, N. J.; LaPointe, N. E.; Kincannon, W. M.; Bleiholder, C.; Feinstein, S. C.; Teplow, D. B.; Buratto, S. K.; Bowers, M. T. Factors That Drive Peptide Assembly and Fibril Formation: Experimental and Theoretical Analysis of Sup35 NNQQNY Mutants. *J. Phys. Chem. B* **2013**, *117*, 8436−8446.
(46) Kabsch, W.; Sander, C. Dictionary of Protein Secondary Structure: Pattern Recognition of Hydrogen-Bonded and Geometrical Features. *Biopolymers* **1983**, *22*, 2577−2637.
(47) Joosten, R. P.; Beek, T. A. H. T.; Krieger, E.; Hekkelman, M. L.; Hooft, R. W. W.; Schneider, R.; Sander, C.; Vriend, G. A Series of PDB Related Databases for Everyday Needs. *Nucleic Acids Res.* **2011**, *39*, D411−D419.
(48) Jeon, J.; Shell, M. S. Charge Effects on the Fibril-Forming Peptide KTVIIE: A Two-Dimensional Replica Exchange Simulation Study. *Biophys. J.* **2012**, *102*, 1952−1960.
(49) de la Paz, M. L.; Goldie, K.; Zurdo, J.; Lacroix, E.; Dobson, C. M.; Hoenger, A.; Serrano, L. De Novo Designed Peptide-Based Amyloid Fibrils. *Proc. Natl. Acad. Sci. U.S.A.* **2002**, *99*, 16052−16057.
(50) Masunov, A.; Lazaridis, T. Potentials of Mean Force between Ionizable Amino Acid Side Chains in Water. *J. Am. Chem. Soc.* **2003**, *125*, 1722−1730.
(51) Chiti, F.; Calamai, M.; Taddei, N.; Stefani, M.; Ramponi, G.; Dobson, C. M. Studies of the Aggregation of Mutant Proteins in Vitro Provide Insights into the Genetics of Amyloid Diseases. *Proc. Natl. Acad. Sci. U.S.A.* **2002**, *99* (Suppl 4), 16419−16426.
(52) Calamai, M.; Taddei, N.; Stefani, M.; Ramponi, G.; Chiti, F. Relative Influence of Hydrophobicity and Net Charge in the Aggregation of Two Homologous Proteins. *Biochemistry* **2003**, *42*, 15078−15083.
(53) Colletiera, J.-P.; Laganowskya, A.; Landaua, M.; Zhaoa, M.; Soriagaa, A. B.; Goldschmidta, L.; Flotb, D.; Cascioa, D.; Sawayaa, M. R.; Eisenberga, D. Molecular Basis for Amyloid-β Polymorphism. *Proc. Natl. Acad. Sci. U.S.A.* **2011**, 16938−16943.
(54) Arnaudov, L. N.; de Vries, R., Theoretical Modeling of the Kinetics of Fibrilar Aggregation of Bovine Beta-Lactoglobulin at pH 2. *J. Chem. Phys.* **2007**, *126*.
(55) Bleiholder, C.; Dupuis, N. F.; Bowers, M. T. Dimerization of Chirally Mutated Enkephalin Neurotransmitters: Implications for Peptide and Protein Aggregation Mechanisms. *J. Phys. Chem. B* **2013**, *117*, 1770−1779.
(56) Yan, Y. B.; Zhang, J.; He, H. W.; Zhou, H. M. Oligomerization and Aggregation of Bovine Pancreatic Ribonuclease A: Characteristic Events Observed by FTIR Spectroscopy. *Biophys. J.* **2006**, *90*, 2525−2533.
(57) Griffith, J. Nature of the Scrapie Agent: Self-Replication and Scrapie. *Nature* **1967**, *215*, 1043−1044.
(58) Harper, J. D.; Lansbury, P. T., Jr. Models of Amyloid Seeding in Alzheimer's Disease and Scrapie: Mechanistic Truths and Physiological Consequences of the Time-Dependent Solubility of Amyloid Proteins. *Annu. Rev. Biochem.* **1997**, *66*, 385−407.
(59) Serio, T. R.; Cashikar, A. G.; Kowal, A. S.; Sawicki, G. J.; Moslehi, J. J.; Serpell, L.; Arnsdorf, M. F.; Lindquist, S. L. Nucleated Conformational Conversion and the Replication of Conformational Information by a Prion Determinant. *Science* **2000**, *289*, 1317−1321.
(60) Calamai, M.; Chiti, F.; Dobson, C. M. Amyloid Fibril Formation Can Proceed from Different Conformations of a Partially Unfolded Protein. *Biophys. J.* **2005**, *89*, 4201−4210.